Electronic Transport

E. Gornik, M. Kast, C. Pacher, G. Ploner, C. Rauch, G. Strasser, J. Ulrich, K. Unterrainer

Institut für Festkörperelektronik, Technische Universität Wien, Floragasse 7, A-1040 Vienna, Austria

A. Neubauer, S. Kaufmann, D. Pum, U. Sleytr
Vienna University of Agriculture

1. Quantum wire photoconductive FIR detectors

(G. Ploner, J. Ulrich, G. Strasser, E. Gornik)

Quasi one-dimensional (1D) conductors or quantum wires are promising devices for photoconductive detection in the far-infrared spectral range. The energetic spacing of their 1D sublevels is typically in the range between 1 – 10 meV, which can be exploited to detect radiation in the corresponding frequency range. One possibility to do this is to investigate the frequency-dependent changes of the wire conductance under FIR radiation. The device principle currently under investigation is shown in Fig. 1.

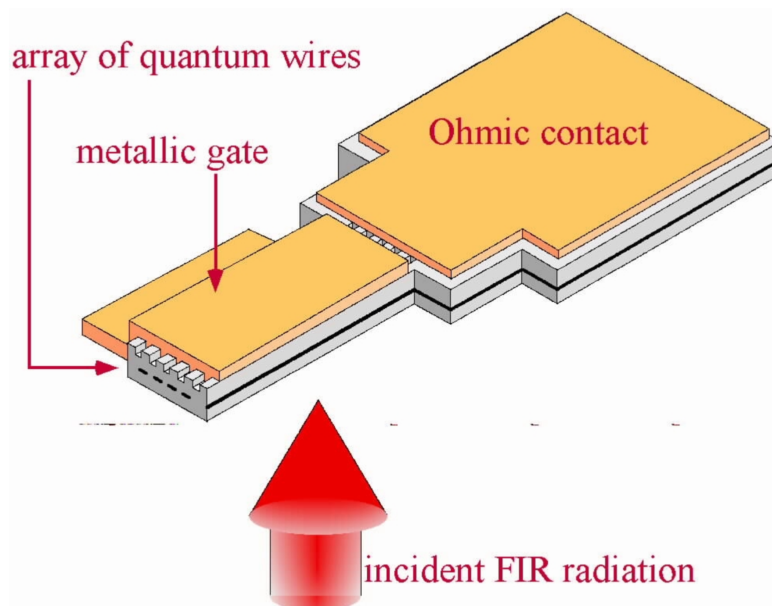

Fig. 1: Quantum wire FIR detector. The metallic top gate used to vary the strength of the lateral 1D confinement potential necessitates that the radiation is coupled into the device from the back side, as indicated by the red solid arrow.

Since previous investigations with side gated single wires have shown that in order to obtain a measurable photoconductive signal it is necessary to have relatively large areas covered with a wire array, we adopt the sample layout indicated in Fig. 1. The wire array is fabricated by shallow etching of 100 – 200 nm wide channels into the surface of the

semiconductor and subsequently covered by a metallic gate. The gate gives the possibility to vary the confinement strength and thus to tune the frequency position of the expected photoconductive signal. Transport measurements show that the sublevel energies of these devices, when fabricated from standard heterostructure material, is in the range of 1 – 2 meV. An alternative, currently implemented approach for wire fabrication consists in structuring some insulating material (e.g. polyimide) into an array of narrow stripes, again followed by covering the resulting structure with a tuning gate.

Figure 2 shows an STM topograph of a typical shallow etched wire array. The roughness of the surface seen in the picture is due to the granularity of a thin Au film deposited on top of the sample prior to the STM imaging.

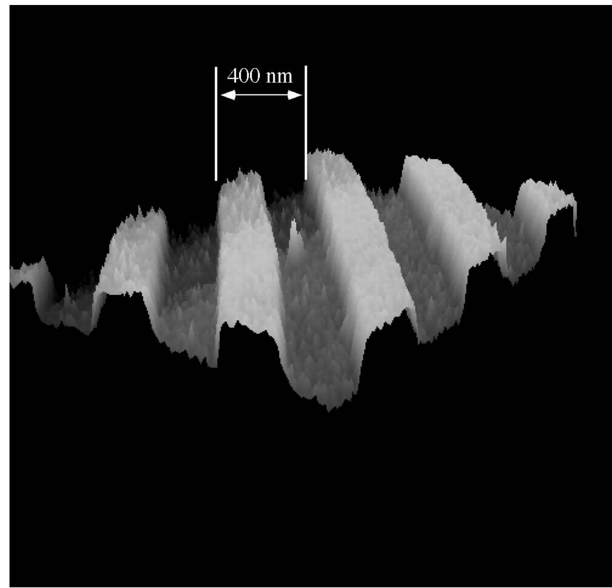

Fig. 2: STM topograph of a shallow etched wire array with 400 nm period.

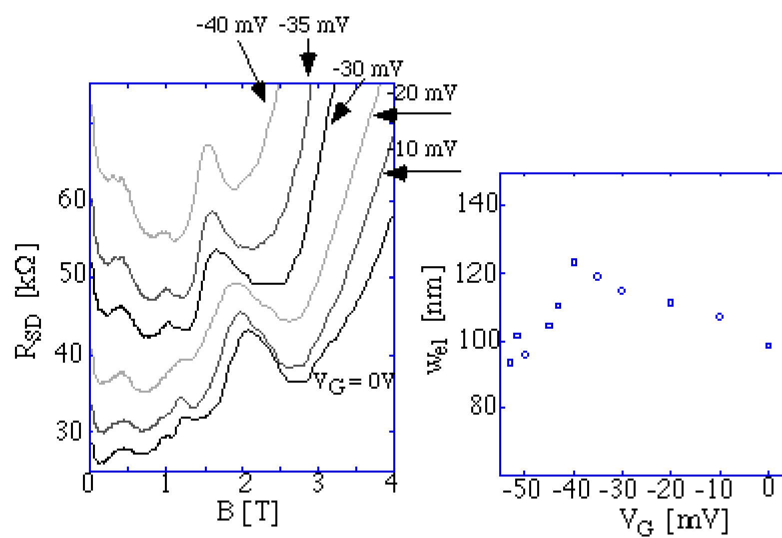

Fig. 3: Magnetotransport data of a gated wire array (left); Variation of the wire width as a function of the top gate voltage VG (right).

Figure 3 shows some typical magnetotransport data for a sample similar to the one depicted in Fig. 1. The magnetoresistance displayed on the left hand side shows the characteristic features of 1D transport. From these curves an estimate for the effective wire width is obtained (right hand side of Fig. 3) along with its dependence on the top gate voltage. Since the wire width is an indirect measure of the subband energies this shows the tuning capability of the gated wire array.

2. Fabrication of 2D lateral superlattices by deposition of bacterial crystalline surface (s-) layers on top of a GaAs-AlGaAs heterojunction

(G. Ploner, E.Gornik; A. Neubauer, S. Kaufmann, D. Pum, U. Sleytr)

In cooperation with the Center of Ultrastructure Research of the Vienna University of Agriculture an attempt is made to use crystalline layers of bio-molecules as templates for nanolithographic processes. These so-called s-layers form, when recrystallized on a semiconductor surface, large arrays of regularly arranged nanopores. The diameter of these pores can be as small as 3 nm; the period of the crystalline arrangement is typically of the order 10 nm. It has been shown that it is possible to deposit metal clusters within these pores. When transferred to the surface of a semiconductor heterostructure, the resulting regular array of metal clusters could be used to induce a weak potential modulation in a nearby two-dimensional electron gas (2DEG), thereby forming a lateral superlattice (SL). We currently investigate the possibility to induce artificial bandstructure in a 2DEG via a grating of Pt/C metal clusters on top of a GaAs-AlGaAs heterostructure that has been arranged into a lateral SL via an s-layer (see the schematics in Fig. 4).

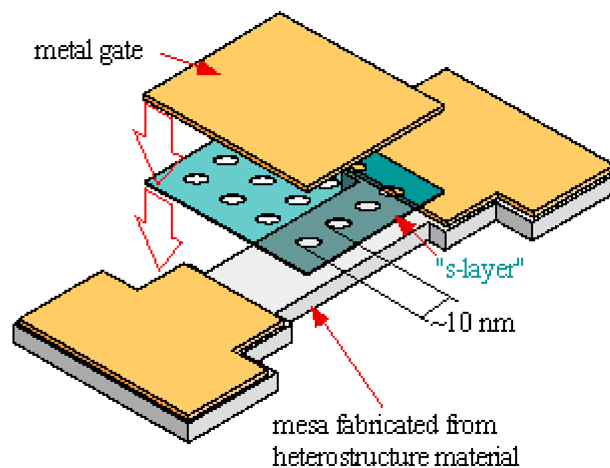

Fig. 4: Schematics of the use of biomolecular s-layers as template for nanofabrication.

We have shown that the required combination of standard lithography with s-layer processing is possible and recently succeeded in depositing a nanocrystalline s-layer on top of a GaAs semiconductor sample. Figure 5 shows an AFM image of the s-layer, which has been deposited on the surface of a GaAs sample within a 4 µm wide photoresist window. The s-layer is seen to form nano-crystals with an average grain size of 100 nm.

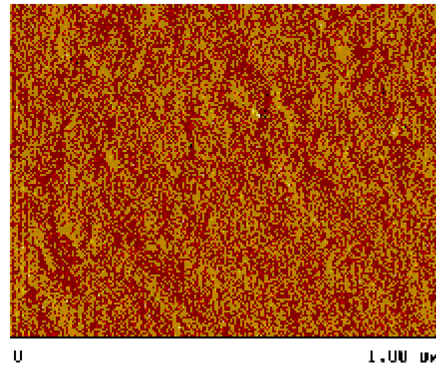

Fig. 5: Contact mode AFM image of an s-layer, deposited on top of a GaAs wafer.

The use of high-mobility material situated close to the sample surface as a substrate for the s-layer superlattice will possibly allow the investigation of band structure effects on the magnetotransport properties or an extensive study of ballistic weak localization effects. These subjects are not easily accessible when the surface superlattice is fabricated by standard lithographic methods, since the currently accessible superlattice periods are in the range of 100 nm. Using s-layers for nanofabrication the SL period could be reduced by an order of magnitude, which would facilitate the experimental investigation.

3. Current spectroscopy of novel GaAs/AlGaAs-heterostructures with three-terminal device technology

(C. Pacher, C. Rauch, M. Kast, K. Unterrainer, G. Strasser, E. Gornik)

Lately we used the three-terminal device technology to demonstrate the transition between coherent and incoherent transport in undoped GaAs/AlGaAs-superlattice minibands. Furthermore we could estimate the coherence length of electrons in this type of superlattice to be approximately 150 nm.

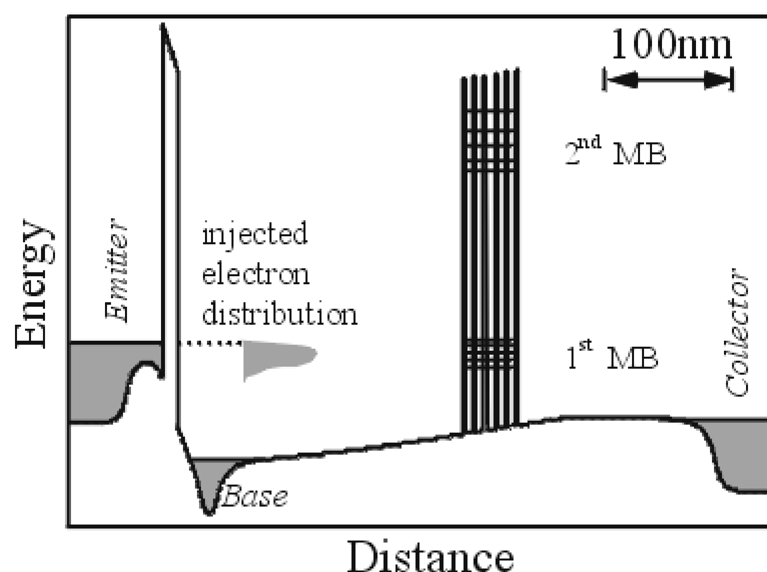

Fig. 6: Band structure of a Three-Terminal Device (5-period superlattice)

The technology of three-terminal devices (3TD) provides the necessary flexibility to study the transmission in dependence of both incident energy and applied electric field across the superlattice. The incident energy can be controlled through the emitter voltage; the collector voltage defines the electric field across the superlattice. The drift region in front of the superlattice reduces resonance effects, which come from the quantum well consisting of the injector barrier and the first barrier of the superlattice.

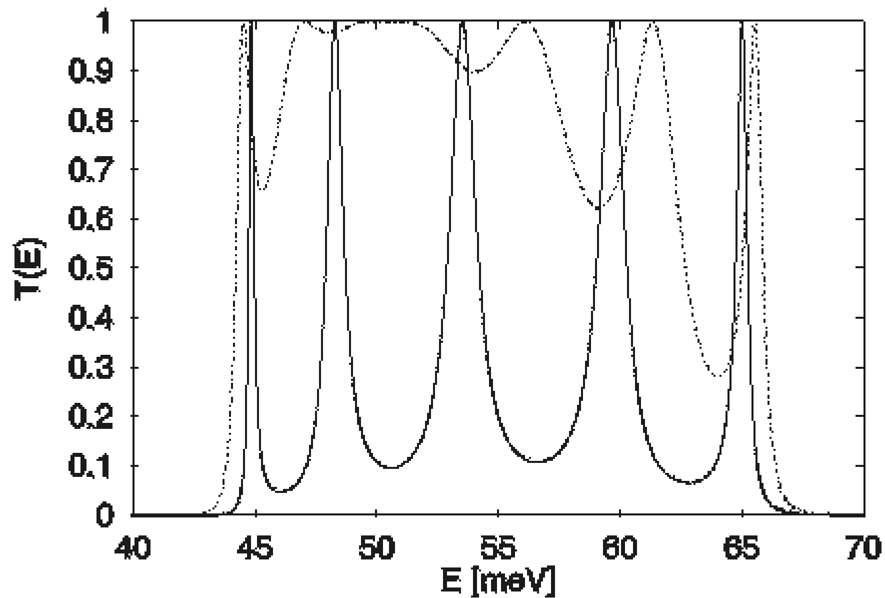

Fig. 7: Transfer-matrix based calculation of transmission through 5-period superlattice (first miniband) with anti-reflection coating (ARC) (dotted line) and without ARC (solid line). (calculations by F. Elsholz, TU Berlin)

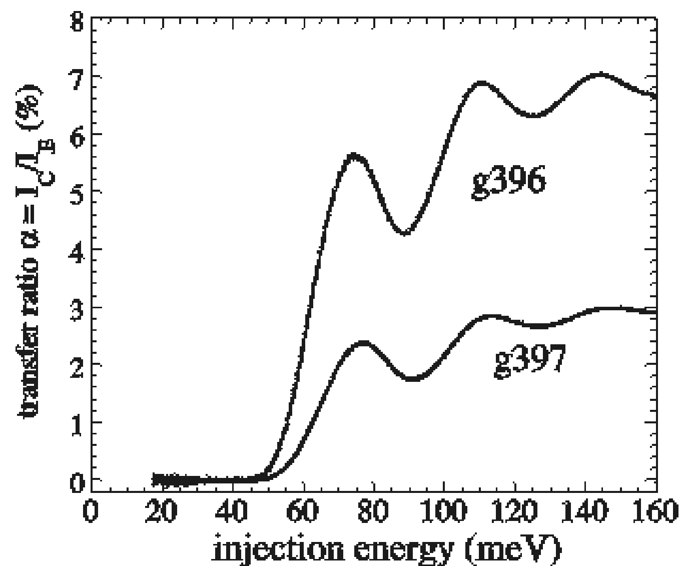

Fig. 8: Experimental data from two 3TDs: 5-period superlattice with (sample g396) and without (g397) anti-reflection coating. The multiple resonances have their origin in ballistic electrons which emitted one or more LO phonons.

The 3TD-technology can also be used to study ballistic transport through (nearly) arbitrary GaAs/AlGaAs heterostructures within a length of the order of 150 nm. We demonstrated the effect of an anti-reflection coating (ARC) for superlattices: an additional barrier with half the width of the superlattice barriers both in front of and after the superlattice increases the integrated transmission through the first miniband by a factor of about 2.5 in very good agreement with a simple transfer matrix calculation.

4. Observation of electron transport in GaAs/AlGaAs superlattices in the presence of crossed electric and magnetic fields

(M. Kast, C. Rauch, G. Strasser, E. Gornik)

In this work we present a study about the influence of crossed electric and magnetic fields on the electron transport in superlattice minibands. A three terminal device is used to probe the transmittance of undoped GaAs/GaAlAs superlattices in crossed electric and magnetic fields. An energy tunable electron beam is generated by a tunneling barrier and passes the superlattice after traversing a thin highly doped base layer and an undoped drift region. The transfer ratio ($=I_c/I_e$) reflects the probability of an injected electron to be transmitted through the superlattice. Electric field is applied across the superlattice and magnetic field perpendicular to the growth direction. Applying an in-plane magnetic field causes a deflection of the electron beam due to the Lorentz force. While the electric field leads to the localization of the electron wave function, the magnetic field increases the total effective electron path in the superlattice. As a result, incoherent transport is observed at positive superlattice bias conditions. The increase of the transfer ratios, at positive superlattice bias, with increasing magnetic field is shown in Fig. 9. We have taken the total miniband transmission, which is defined as twice the area of the lower energy side of the first transfer ratio peak, as a measure for the average current through the first miniband at given bias conditions. The change in the asymmetric behavior of the miniband-transmission, due to the increase of the total effective electron path in the superlattice, is shown in Fig. 10.

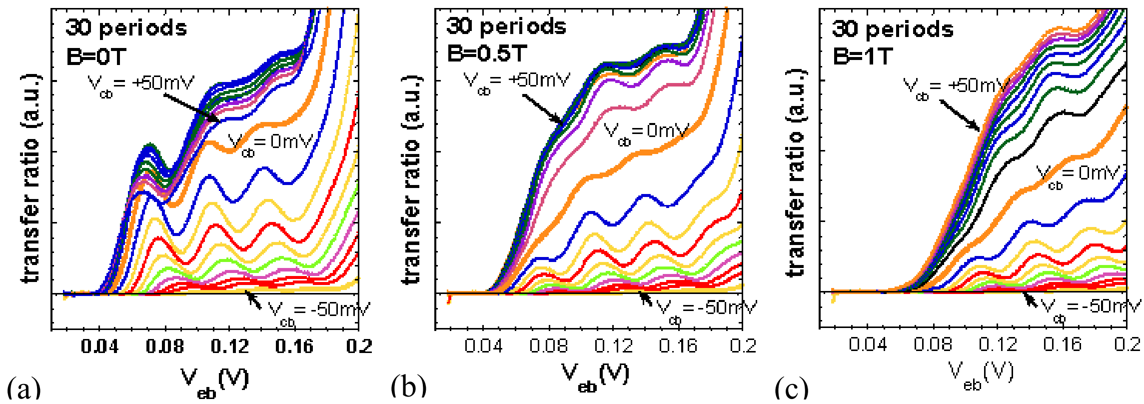

Fig. 9: Transfer ratios of a 30 periods superlattice at B = 0 T (a), B = 0.5 T (b) and B = 1 T (c).

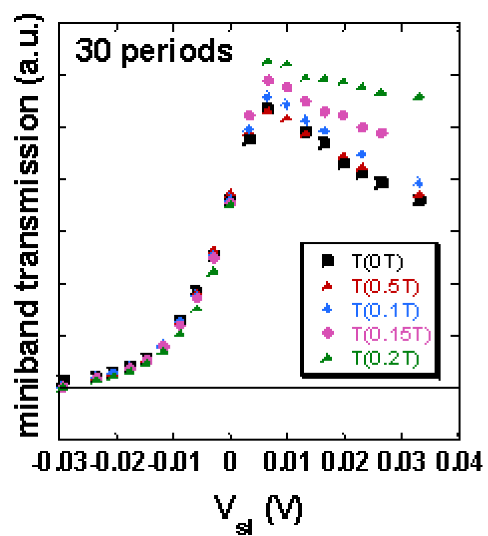

Fig. 10: Miniband transmission at various magnetic fields